



LAWRENCE
LIVERMORE
NATIONAL
LABORATORY

Surface Chemistry of GaP(001) and InP(001) in Contact with Water

B. C. Wood, E. Schwegler, W. Choi, T. Ogitsu

September 27, 2013

Journal of Physical Chemistry C

Disclaimer

This document was prepared as an account of work sponsored by an agency of the United States government. Neither the United States government nor Lawrence Livermore National Security, LLC, nor any of their employees makes any warranty, expressed or implied, or assumes any legal liability or responsibility for the accuracy, completeness, or usefulness of any information, apparatus, product, or process disclosed, or represents that its use would not infringe privately owned rights. Reference herein to any specific commercial product, process, or service by trade name, trademark, manufacturer, or otherwise does not necessarily constitute or imply its endorsement, recommendation, or favoring by the United States government or Lawrence Livermore National Security, LLC. The views and opinions of authors expressed herein do not necessarily state or reflect those of the United States government or Lawrence Livermore National Security, LLC, and shall not be used for advertising or product endorsement purposes.

Surface chemistry of GaP(001) and InP(001) in contact with water

Brandon C. Wood,^{1, a)} Eric Schwegler,¹ Woon Ih Choi,¹ and Tadashi Ogitsu¹
*Quantum Simulations Group, Lawrence Livermore National Laboratory, Livermore,
 CA 94550*

We report the results of total-energy density functional theory and *ab initio* molecular dynamics simulations of (001) surfaces of InP and GaP in contact with gas-phase and liquid water. Both pristine and oxygen-rich surfaces (representing a submonolayer native surface oxide) are considered. We find that gas-phase binding of water on pristine mixed-dimer $\delta(2 \times 4)$ reconstructions of InP/GaP(001) is comparable to the solvation energy of liquid water, and that the barriers for room-temperature dissociation are high. In the presence of a submonolayer surface oxide, water binding and dissociation instead become strongly exothermic, and proceed with almost no barrier. In this case, the surface chemistry at the interface with liquid water differs significantly from that of gas-phase water adsorption due to the formation of strong interfacial hydrogen bonds between surface adsorbates and water molecules. Water dissociation on the oxygen-rich surface is accompanied by extremely rapid local proton hopping between hydrogen-bonded surface adsorbates.

I. INTRODUCTION

Photoelectrochemical production of H_2 fuel from water and sunlight represents a promising long-term, sustainable energy solution.¹ However, development of an electrode material that meets targets for both efficiency and durability has proven extremely challenging. The design difficulty arises from the materials requirements that must be simultaneously met, including efficiency of photon harvesting, as well as favorable thermodynamics and reaction kinetics for photolysis.^{2,3} At present, the most efficient devices are based on Group III-phosphide semiconductors. For example, tandem devices based on a GaInP₂ photocathode have demonstrated solar-to-hydrogen conversion efficiencies in excess of 12%.⁴ Unfortunately, these same devices exhibit rapid photocorrosion in aqueous environments, limiting their practicality.⁴⁻¹⁰

Ab initio modeling and simulation can provide unique insight into the chemical mechanisms operating at a III-V surface in contact with water.¹¹⁻¹⁴ Such information is extremely useful for diagnosing limiting factors in electrode stability and performance. To the extent possible, the models should account for the surface and interface structures found in operating devices. For instance, liquid water may influence hydrophilic electrode surfaces differently from gas-phase adsorption. Also, surface adsorbates from atmospheric or electrochemical exposure are ubiquitous in experiments^{8,15-18} but usually neglected in simplified models. These are often oxygen derived, and fundamentally change the surface states and adsorption mechanics under operation.^{7,17-22}

In order to provide a deeper understanding of the influence of water on III-V photoelectrochemical electrode surfaces, we have used density functional theory to perform total-energy calculations and *ab initio* molecular dynamics simulations on model GaP(001) and InP(001) surfaces in contact with water. In so doing, we review and extend our previous work examining InP in the presence

of water,²³ as well as high-vacuum studies of InP(001) and GaP(001) reconstructions in the presence of oxygen and hydroxyl adsorbates.²⁴ The simulations compare how GaP(001) and InP(001) respond to liquid- and gas-phase water, both for pristine surfaces and for surfaces in the presence of a submonolayer native surface oxide.

Whereas this paper focuses on how water impacts the surface structure and chemistry, a companion paper²⁵ addresses how the liquid water structure itself is altered when the full semiconductor-water interface is considered. In that work, we showed that subtle differences in the electronic structure of GaP(001) and InP(001) give rise to very different hydrogen-bond dynamics and topology when the full solvent is considered, which we suggested has implications for the photoelectrochemical performance of electrodes based on these materials. These two studies together constitute a fundamental investigation of the properties of model polar hydrophilic surfaces in aqueous environments.

II. COMPUTATIONAL DETAILS

Total-energy density functional theory calculations and Car-Parrinello molecular dynamics simulations²⁶ were performed using the Quantum-ESPRESSO code²⁷. Ultrasoft pseudopotentials²⁸ were used, with semi-core d states included in the indium and gallium valence descriptions. Wave function and charge density cutoffs of 30 Ry and 300 Ry were used. The Perdew-Burke-Ernzerhof (PBE) exchange-correlation functional²⁹ was adopted, since it provides a good description of hydrogen-bonded systems³⁰. The dynamics simulations used a fictitious electronic mass of 700 a.u. and a time step of 12 a.u., with deuterium substituted for hydrogen to permit the larger values. Simulations were run in the canonical NVT ensemble at 400 K in order to reproduce the structural properties of ambient liquid water.³¹ Temperatures were maintained using Nosé-Hoover chains.³²

The (001) semiconductor slab was generated using seven semiconductor layers with 16 atoms per layer (a (4×4) cell), plus surface atoms (i.e., oxygen or a Ga/In-

^{a)}Electronic mail: brandonwood@llnl.gov

P dimer). Supercell axes were aligned along the $[110]$, $[\bar{1}10]$, and $[001]$ directions. Periodic boundary conditions were imposed in all directions, with top and bottom layers identically terminated to minimize spurious interactions between repeated images. Exposed surfaces were assumed to be In/Ga-rich, motivated by the preferential oxygenation of this surface over the P-rich surface²². Supercell lattice parameters parallel to the slab were 15.57 and 16.91 Å for GaP and InP, respectively.

For the calculations involving gas-phase water, an additional 12 Å of vacuum spacing was included perpendicular to the semiconductor slab, with the Effective Screening Medium Method³³ applied to screen long-range dipolar interactions in the non-repeating direction. To generate the interface with liquid water, the spacing between periodic slab images was increased on 1.65 nm, with enough water molecules (~ 160) inserted so as to recover the experimental density of liquid water in the region center. Initial configurations were derived using pre-equilibrated classical TIP4P-generated bulk water³⁴, placed at the interface and re-equilibrated for 1 ps of *ab initio* dynamics with the surface degrees of freedom frozen. An additional 3.5 ps of equilibration was then performed with full degrees of freedom. Production runs were 20 ps, with statistics averaged over the top and bottom surfaces of the semiconductor slab.

For both InP and GaP, two representative water/semiconductor interface simulations were run. The first was a pristine (001) surface exhibiting the mixed-dimer $\delta(2 \times 4)$ reconstruction commonly observed for the In/Ga-rich (001) surface under ultra-high vacuum.³⁵ The second surface was constructed with surface $M-O-M$ bridges, with oxygens occupying every other bridge site along $[\bar{1}10]$ (0.5 ML coverage). The latter configuration and accompanying coverage were derived from our earlier stability analysis.²⁴ Figure 1 shows the models we used for the pristine and oxygenated GaP/InP(001) surfaces.

III. RESULTS

A. Pristine mixed-dimer $\delta(2 \times 4)$

In Ref.¹², Jeon *et al.* performed a detailed study of gas-phase molecular adsorption of water on the metal-rich mixed-dimer $\delta(2 \times 4)$ reconstruction of GaP(001). They found three adsorption sites for water molecules, corresponding to the three unique undercoordinated Ga atoms in the surface layer. These atoms act as Lewis acids, accepting lone pairs from the oxygen of water. Calculations for molecular binding at each of three candidate sites were repeated for GaP(001) and InP(001), and are presented in Table I. As reported by Jeon *et al.* for GaP(001),¹² the lowest-energy molecular adsorption site on GaP(001) is found to be the Ga atom in the mixed dimer (C), to which the oxygen of the water molecule binds with an energy of -0.40 eV. For InP(001), we find that the A dimer site is more stable,

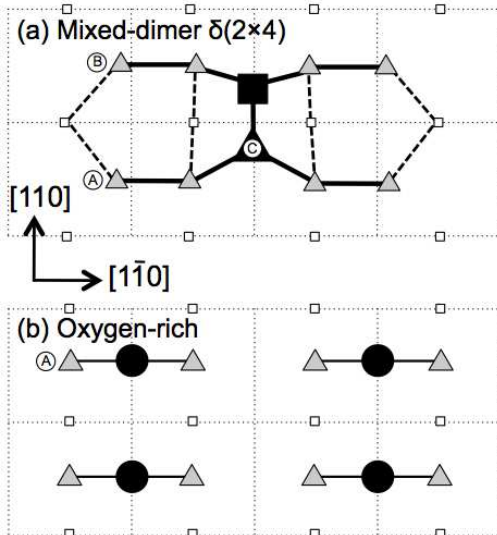


FIG. 1. Surface structural models used in the present study: (a) the mixed-dimer $\delta(2 \times 4)$ reconstruction of the pristine surface; and (b) the oxygen-rich surface with 0.5 ML coverage of bridge oxygens. Triangles, squares, and circles represent In/Ga, P, and O atoms. Larger size and darker color indicates closer proximity to the viewer. The symmetry-inequivalent water binding sites for gas-phase adsorption of water molecules are shown as circled letters. The A , B , and C sites correspond to the 4G, 3G, and 2G sites in Ref.¹².

with a binding energy of -0.38 eV. Both values are comparable to the solvation energy of a water molecule in the liquid phase (-0.42 eV, based on the enthalpy of vaporization).³⁶ Also, all tested sites have adsorption energies within 50 meV of one another, suggesting any of these sites might be accessible at room temperature.

We also investigate the possibility of dissociative water adsorption on the mixed-dimer site (C). This is the most likely dissociation site, since both the phosphorus and the Ga/In are nominally undercoordinated. In this scenario, phosphorus (the Lewis base) can host a proton and Ga/In (the Lewis acid) can host a hydroxyl. Other arrangements are possible, but single-stage decomposition requires a straightforward kinetic pathway in which the dissociation products are physically close (this same conclusion was reached by Jeon *et al.* in their analysis¹²). We find that dissociative adsorption is energetically favored over molecular adsorption for GaP (by 0.20 eV), whereas InP weakly favors molecular adsorption (by 0.12 eV). The calculated results are summarized in Table I. We note that our binding energies and dissociation energies are in reasonable agreement with those reported by Jeon *et al.*¹², with differences likely attributable to subtle differences in bottom-layer terminations, dipole correction schemes, and slab thicknesses.

We also investigated the reaction kinetics for dissociative adsorption, by using the nudged elastic band (NEB) method to calculate barriers for dissociation on

TABLE I. Site-dependent molecular (E_{mol}) and dissociative (E_{diss}) binding energies of a gas-phase water molecule on pristine mixed-dimer $\delta(2 \times 4)$ and oxygen-adsorbed GaP/InP(001). The corresponding NEB-derived kinetic barriers for gas-phase surface water dissociation (ΔE_a) are also given. ΔF_{mol} represents the free-energy difference (taken with respect to the A site) between molecular water binding sites during the liquid water dynamics.

Surface	Site ¹	E_{mol} ² (eV)	ΔF_{mol} ³ (eV)	E_{diss} ^{2,4} (eV)	ΔE_a (eV)
InP $\delta(2 \times 4)$	A	-0.38	0	--	--
InP $\delta(2 \times 4)$	B	-0.34	+0.017	--	--
InP $\delta(2 \times 4)$	C	-0.36	+0.018	-0.24	0.82
GaP $\delta(2 \times 4)$	A	-0.38	0	--	--
GaP $\delta(2 \times 4)$	B	-0.35	+0.013	--	--
GaP $\delta(2 \times 4)$	C	-0.40	+0.014	-0.60	0.71
InP (O-rich)	A	-0.65	--	-1.26	0.04
GaP (O-rich)	A	-0.71	--	-1.25	0.16

¹See Fig. 1 for site designations.

²Negative energies imply exothermic processes.

³Calculated using Eq. 1.

⁴For the mixed-dimer $\delta(2 \times 4)$ surface, dissociation is assumed to occur on the M - P surface dimer, with OH binding to the M site, and H to the P site. For the O-rich surfaces, the mechanism of Fig. 3a-c is assumed.

the mixed-dimer site. The results, listed in Table I, show that water dissociation has a relatively high kinetic barrier (0.82 eV for InP; 0.71 eV for GaP), and is therefore unlikely to proceed unaided.

In order to assess any differences between the properties of the surface with gas-phase water adsorption and with actual liquid water, we performed molecular dynamics simulations of the full interface of the mixed-dimer $\delta(2 \times 4)$ surface with water. As expected based on the high dissociation barriers, all adsorbed water molecules are molecularly rather than dissociatively adsorbed. The available binding sites match those of the gas-phase calculations, with all three symmetry-inequivalent sites (A , B , C) showing evidence of molecular water adsorption (Fig. 2). This agrees with the close energetics of water binding on the three sites.

For the interface with liquid water, we can use the relative probability contours in Fig. 2 to estimate the average free energy difference between binding sites during the dynamics runs. Assuming the system is equilibrated, we compute the difference $F_A - F_B$ between sites A and B according to:

$$F_A - F_B = -k_B T \ln \left(\frac{n_A}{n_B} \right), \quad (1)$$

where n represents the relative probability of binding at the given site. Using this formula on the dynamics trajectories of the water-semiconductor interface gives the free energy differences shown in Table I. The free en-

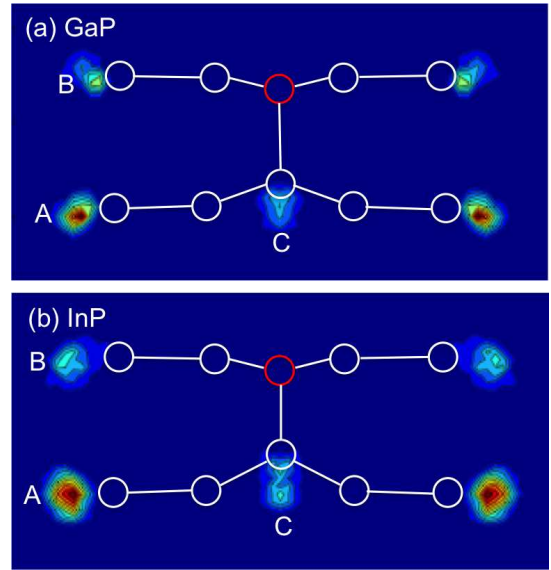


FIG. 2. Probability contours showing preferred molecular adsorption sites of liquid water on the mixed-dimer $\delta(2 \times 4)$ reconstruction of (a) GaP and (b) InP during the course of the dynamics simulations. Red indicates the highest-probability location of the water oxygen. White and red circles indicate the atomic positions of surface In/Ga and P atoms, respectively. A water molecule was considered adsorbed if the In/Ga-O bond was shorter than the first minimum in the corresponding radial pair distribution function (not shown).

ergies of binding are indeed very close for each of the sites, as expected from the analogous gas-phase water calculations. However, the A site is more stable than the mixed-dimer site (C), which is the opposite of what we found in the gas-phase calculations. In addition, further analysis of the probability density of binding near site C in the dynamics (Fig. 2) reveals a different configuration from what we calculated for gas-phase adsorption. In the gas-phase calculation, the proton in water interacts with the lone pair on the phosphorus. This reorients the water molecule such that its oxygen sits almost directly atop the In/Ga atom in the mixed dimer. On the other hand, in the liquid dynamics, the probability density is smeared away from the phosphorus. This resembles an alternate configuration considered by Jeon *et al.*, in which the proton-phosphorus interaction is broken. That configuration was found to be less favorable for gas-phase water adsorption on GaP(001) than the case where the proton-phosphorus interaction is intact. However, it was also found to have a binding energy intermediate between the A and B sites, which agrees with the ordering we find in the dynamics of the interface with liquid water. The lack of proton-phosphorus interaction in the dynamics is most likely due to unfavorable energetic and entropic competition with respect to hydrogen bonding with other water molecules in the solvent. This explanation is consistent with the higher electronegativity of oxygen with

respect to phosphorus, which translates to higher polarization in an O–H bond of water than in a Ga/In–P surface bond, and therefore to stronger hydrogen bonding with the former.

B. Sub-monolayer surface oxide

We previously developed a bond-topological model to categorize oxygen adsorption based on its immediate chemical environment, and showed that this provides an adequate descriptor for key features in the electronic and atomic structure of our model surfaces.²⁴ We concluded that model surfaces could be constructed based on the most common bond topologies in order to generalize results to more complex compositions and morphologies. Here, we have used those insights to construct a model oxygen-rich surface that mimics nucleation of a sub-monolayer surface oxide on (001)-oriented GaP/InP. The surface is derived from the M –O– M bridge oxygen topology, which forms primarily at the metal-rich polar (001) surface.²⁴

The addition of oxygen-derived surface adsorbates dramatically changes the electronic and chemical properties of the metal-rich (001) surfaces of InP and GaP, as we reported in Refs.²³ and²⁴. Among other effects, the changes cause significant enhancement of water dissociation at the surface oxygen bridge site. This is observed in both gas-phase and liquid dynamics simulations; however, as discussed below, the explored mechanisms and reaction energetics are substantially different when liquid water is present. There turns out to be two primary drivers for this behavior: first, surface dipole enhancement leading to higher proton affinity; and second, the ability of oxygen derivatives to form direct hydrogen bonds with water.

We begin with a discussion of gas-phase water binding. The calculated energies for molecular and dissociative binding of gas-phase water on O-rich InP(001) and GaP(001) are listed in Table I. The addition of surface oxygen significantly stabilizes both molecular adsorption (by > 0.3 eV) and dissociative adsorption (by 0.6–1.0 eV) with respect to binding on the pristine surface. Dissociative adsorption is particularly stable, being universally more favorable than molecular adsorption on the oxygen-rich surface.

In dissociative adsorption on O-rich InP/GaP(001), the surface oxygen acts as the proton acceptor to form hydroxyl. The remaining hydroxyl group is left behind on the neighboring In/Ga site. Because oxygen has a much higher proton affinity than does phosphorus (the proton acceptor on the pristine surface), dissociation becomes relatively more stable. In the case of molecular adsorption, the stabilization with respect to the pristine surface is instead a direct consequence of the capability of the adsorbed water molecule to form hydrogen bonds with the surface oxygen. It is worth noting that based on the degree of molecular adsorption stabilization (> 0.3 eV), this

hydrogen bonding appears to be unusually strong compared to the reported hydrogen-bond strengths in water dimers and in liquid water of about 0.16 eV and 0.24 eV, respectively.^{37,38}

Comparing dissociative adsorption of gas-phase water on GaP to InP, Table I shows that the energetics are in fact very similar. This is in sharp contrast to the pristine surface, where dissociative adsorption on O-rich GaP is strongly favored over O-rich InP. The similarity can be understood in light of the hydroxyl product complexes that arise from water dissociation at the bridge oxygen site. As we showed in Ref.²⁴, binding of hydroxyl adsorbates on GaP/InP(001) is comparatively ionic in nature, and therefore depends only weakly on the specific electronic-structure differences between GaP and InP. Accordingly, the dissociation energy total formation energy of the product complex gives a nearly identical value for the two surfaces (1.26 eV for InP versus 1.25 eV for GaP).

Table I also reports the estimated barriers for dissociation of a molecularly adsorbed gas-phase water molecule on oxygen-rich GaP/InP(001), as calculated using the NEB method. The strongly exothermic nature of water dissociation on these surfaces correlates to very low dissociation barriers of 0.04 eV and 0.16 eV for InP and GaP, respectively. The thermodynamic and kinetic favorability dissociative adsorption suggests that any surface oxygen is likely to convert readily to surface hydroxyl when immersed in water. We point out that the values in Table I represent total energies rather than Gibbs free energies, and that changes in pH or electrical potential will certainly shift the thermodynamic equilibrium; nevertheless, the thermodynamic driving force for surface hydroxylation seems clear.

We turn now to the dynamics of the interface of O-rich GaP/InP(001) with liquid water. As expected based on the low calculated activation barriers for gas-phase dissociation, we are able to directly observe water dissociation events in the liquid dynamics. One such event, which follows the same reaction pathway as gas-phase dissociation, is shown in detail in Fig. 3a–c. It is a local event in which both the proton donor and acceptor are anchored to the same In/Ga atom. The oxygen of the water molecule binds to the edge of the M –O– M bridge, with one O–H forming a hydrogen bond with the bridge oxygen. The hydrogen bond rotates the water dipole away from the surface normal direction, aligning the O–H \cdots O complex and shortening the proton-transfer path.

However, we also find that the presence of liquid water activates a second mechanism for dissociative adsorption of water on M –O– M bridges on GaP(001) or InP(001), this time connected to the formation of Grotthuss chains involving solvent water molecules. This second mechanism was first reported for InP in Ref.²³, and is shown in Fig. 3d–f. In this case, proton donor and acceptor oxygens are bound to different In/Ga atoms, and connected by a Grotthuss chain³⁹ involving a water molecule in solution. The chain has a low barrier for proton dif-

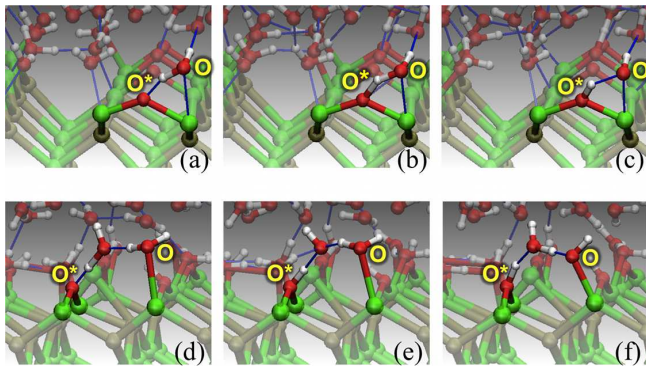


FIG. 3. Two alternative mechanisms for water dissociation at surface oxygen bridges, as observed in the dynamics simulations of the full interface of InP(001) with liquid water. O and O* refer to proton donor and acceptor oxygens, respectively. (a–c) The first scenario features a donor water molecule bound to one of the edge In atoms adjacent to O*, and transferring a proton across the O–H···O* complex. (d–f) The second scenario has the donor water molecule bound to an In atom that is not part of the In–O*–In bridge. In this instance, water molecules in solution act as intermediaries in a Grotthuss chain for site-to-site proton transfer. Color scheme: O=red, H=white, In=green, P=gray.

fusion, which proceeds via the Grotthuss mechanism as coordinated jumps across successive O–H···O complexes. Overall, this second mechanism (Fig. 3d–f) exhibits more commonly than the first (Fig. 3a–c) in the course of the dynamics.

Water dissociation via both of the mechanisms in Fig. 3 appears to be reversible at the interface with liquid water. Surprisingly, this is even true for the first mechanism in Fig. 3a–c: although much rarer than the forward reaction in this case, we nevertheless directly observe deprotonation of surface M –[OH]– M bridges to reform M –O– M in the course of the dynamics simulations. This means that both the protonation and deprotonation reactions are kinetically and thermodynamically accessible within the physical conditions of interest and the timescales of the simulation dynamics. This is particularly unexpected considering that M –[OH]– M bridge hydroxyls are found to be significantly more stable than M –O– M bridges *in vacuo*, as detailed in Ref.²⁴ and suggested by the results of Table I. This confirms the importance of hydrogen bonding in determining the free energies of these structures in liquid water with respect to their gas-phase counterparts.

The result of both water dissociation mechanisms is local hydroxylation of the initially oxygen-rich surface, with the original water site now carrying a dangling-bond atop hydroxyl (M –OH), and the target site carrying a bridge hydroxyl (M –[OH]– M). Schematically, they can be written as:



Accordingly, in the absence of competing pathways, the initial presence of oxygen bridge topologies should lead to preferential surface hydroxylation in water. This is similar to the common behavior of oxide surfaces.⁴⁰

The local proton-transfer events that accompany water dissociation on the oxygen-rich surfaces are extraordinarily frequent in the dynamics of the interface with liquid water, confirming the low barrier for dissociation listed in Table I. We note that similar local proton-hopping behavior has been observed theoretically and experimentally in the context of several other interfacial systems.^{13,41–49} Interestingly, GaP demonstrates a proton-hopping rate that is about twice that of InP, suggesting some differences in the relative hydrogen-bond strengths of water at the two surfaces that are not reflected in the gas-phase calculations of Table I. As is explored in detail in a companion paper,²⁵ these differences turn out to have key additional implications for the hydrogen-bond network dynamics of liquid water near the two interfaces. Among the unexpected consequences is that once these implications are taken into account, the GaP(001)-water interface actually exhibits *slower* long-range surface proton transport behavior, despite its faster local, site-to-site proton hopping rate.

In order to explore the underlying chemical motivation for the unusually high rate of surface local proton hopping on the oxygen-rich surface, we have used the method of maximally localized Wannier functions (MLWFs)⁵⁰ to extract and analyze the electronic structure. The calculation of MLWFs is analogous to the use of the Boys localization method in quantum chemistry,⁵¹ and minimizes the spatial extent of the orbitals under a unitary transformation of the basis. The location of the Wannier function center (WFC) gives information about the relative ionicity or covalency of a bond, since ionic bonds tend to have ion-centered WFCs, whereas covalent bonds tend to have bond-centered WFCs. WFCs can also be used to determine bond polarization and to calculate dipole moments. In addition, the minimum spread gives information about the relative localization of the electronic density. MLWFs were calculated for all interfacial water molecules within 15 uncorrelated frames, each separated by 1 ps of simulation time. For simplicity, we include in our analysis only molecularly adsorbed water, thereby deliberately neglecting the dissociation events.

MLWFs were used to calculate the average water dipole moments in at the interface with the liquid, based on the vector sum of the nuclear coordinates and WFCs. The results show a significant enhancement of the average dipole moment of a liquid water molecule once it molecularly adsorbs on the oxygen-rich InP/GaP(001) surface. This is a response to the surface dipole induced by the additional oxygen. Specifically, the computed value goes from 3.0 Debye in the bulk-like water region midway between surface slab images to 4.5 Debye at oxygen-rich InP(001) and 4.8 Debye at oxygen-rich GaP(001). This represents an enhancement of 50% or more, signaling a fundamental shift in the water electronic structure in this

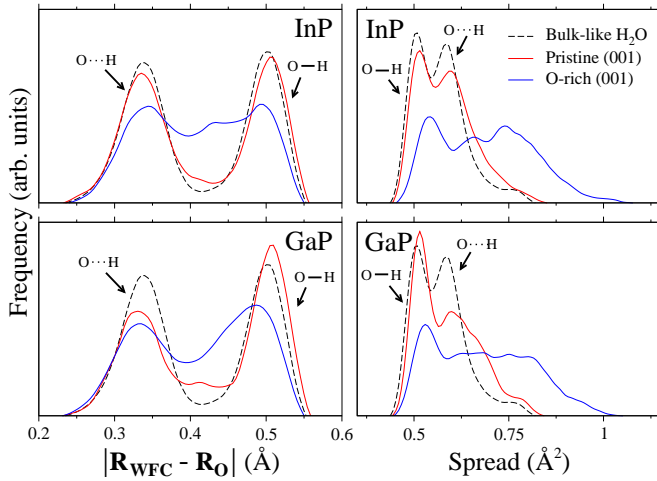


FIG. 4. Distribution of the centers (left) and spreads (right) of the maximally localized Wannier functions associated with oxygens of molecular water adsorbed on the surface during the course of the interface dynamics. Separate distributions are shown for pristine mixed-dimer $\delta(2 \times 4)$, O-rich, and OH-rich InP(001) (top) and GaP(001) (bottom). The dashed line is the value for the bulk-like water region midway between periodic surface images.

region. For comparison, we also calculated the average dipole moment of molecularly adsorbed water on the pristine mixed-dimer $\delta(2 \times 4)$. In this case, we observed a much more modest 10% increase in the dipole moment, to 3.2 and 3.3 Debye for InP(001) and GaP(001), respectively.

Accompanying the dipole enhancement at the interface with liquid water is a reorganization of the charge density of adsorbed water molecules. This can be seen upon examination of the distributions of WFCs and spreads for water oxygens adsorbed on the surface during the dynamics, shown in Fig. 4. For reference, distributions for bulk water feature two peaks: shorter spreads and longer distances between nuclei and Wannier functions are associated with O–H chemical bonds, and vice versa for nonbonded/hydrogen bond-acceptor oxygen electron pairs. However, Fig. 4 shows that addition of surface O tends to break down the bimodality, blurring the electronic distinction between O–H chemical and O···H hydrogen bonds. The distribution of spreads also broadens significantly, indicating increased delocalization of electrons across chemical and hydrogen bonds. Taken together, these effects point to decreased covalency in the O–H chemical bonds, accompanied by increased O···H hydrogen-bond strength. Weaker chemical bonds and stronger hydrogen bonds translates to a low barrier for Grotthuss-type exchange between the two,³⁹ thereby driving the frequent surface local proton transfer events.

In contrast with the oxygen-rich surface, Fig. 4 shows that the pristine mixed-dimer $\delta(2 \times 4)$ surface in contact with liquid water largely retains the bimodal distributions found in the bulk-like region of the water. How-

ever, the pristine surface also carries a significant surface dipole. We therefore conclude that the observed changes in the molecular and electronic structure of adsorbed water on the oxygen-rich surface are not merely dipole induced. Rather, they reflect an unusually strong surface hydrogen bonding with adsorbates and with neighboring water molecules, which is largely absent for the pristine surface. This manifests as dramatically increased hydrophilic character, which profoundly influences the structure and chemistry of the interface.

IV. DISCUSSION

The fact that we do not observe dissociative adsorption of either liquid or gas-phase water on the pristine surface suggests that a surface adsorbate is necessary for favorable dissociation kinetics on InP(001) or GaP(001) at zero bias. In this respect, our surface oxygen results are consistent with simulations of water dissociation on InP(100) in the presence of surface hydrogen.¹¹ However, this behavior differs from the (110) surface of GaP/InP, where water dissociation reportedly proceeds unaided.^{13,52}

Recently, May *et al.* presented detailed photoelectron spectroscopy results that point to a combination of dissociatively and molecularly adsorbed water when the Ga-rich mixed-dimer (2×4) reconstruction of GaP(001) is exposed to water vapor.^{18,53} Because dissociative adsorption on pristine GaP(001) should be comparatively rare due to the high kinetic barrier, we suggest that these observations are more likely the result of a two-stage process. First, oxygen or hydroxyl is probably deposited by a high-barrier water dissociation event, or else by direct surface adsorption. This surface site then becomes available for water dissociation via a low-barrier process. Once the cycle begins, the dissociation products remain as sites for possible further low-barrier water dissociation, ensuring that a sizeable concentration of dissociated water will eventually exist at the surface.

Similarly, our dynamical simulation results allow us to speculate about the likely reactions that govern the immediate interfacial chemistry of InP/GaP(001) in a photoelectrochemical cell, where the semiconductor is in full contact with liquid water. Prior to illumination, surface oxygen bridges are created through exposure to air or water. Upon immersion, these act as proton acceptors to promote dissociative adsorption of water molecules, thereby depositing additional oxygen and hydroxyl on the surface. This probably occurs via one of the low-barrier dissociation pathways enabled by hydrogen-bond interactions between the adsorbate and the solution. Under efficient cathodic operation, protons will be rapidly consumed via the evolution of H_2 gas. Depending on the active mechanism, the source of these protons could either be the surface itself, or else the solution (which will subsequently be rendered locally basic with respect to the bulk). Either way, the likely effect will be to encourage

surface deprotonation. Because the simulations show deprotonation of surface hydroxyl groups to be kinetically feasible at room temperature via the reverse reaction of Fig. 3d–f, we assume that device operation will enhance the continuous regeneration of oxygen sites that can be used for further water dissociation. Accordingly, we propose that even small initial concentrations of surface oxygen will tend to nucleate dense surface hydroxylation via the mechanisms shown in Fig. 3.

Previous reports in the literature have highlighted the favorable role of surface oxygen adsorption in enhancing the stability and kinetics of InP-based cells in an aqueous electrolyte.^{6,19,21,54–56} The stabilizing behavior has been attributed to the passivation of surface states that can act as recombination sites. In these reports, surface oxygen was often proposed as the passivating agent. However, surface oxygen is generally hydroxylated in our simulations; in this case, the passivation of individual surface sites is more likely to be driven by surface hydroxyl groups interacting strongly with interfacial water.

As a final note, we have shown that water dissociation at the oxygen-rich surface is accompanied by local site-to-site proton transfer of the sort shown in Fig. 3. However, there is a subtle but important distinction between such local hopping and actual long-range hydrogen transport. Specifically, local hopping will translate into long-range transport (i.e., the possibility of a surface protonic current) only if the involved hydrogen-bonded complexes can reorganize themselves dynamically between proton-transfer events. The variation in the donor-acceptor combinations guarantees topological diversity, ensuring that the proton does not simply hop back and forth between a small number of similar configurations. This highlights the importance of the structure and dynamics of the hydrogen-bond network, which are explored at length in Ref.²⁵.

V. CONCLUSIONS

In conclusion, we have used density functional theory and *ab initio* molecular dynamics simulations of InP(001) and GaP(001) to investigate how the surface structure and chemistry changes upon contact with water. On the pristine mixed-dimer $\delta(2 \times 4)$ surface, both molecular and dissociative adsorption of gas-phase water molecules are thermodynamically possible, although the high calculated barrier for dissociation (0.71–0.82 eV) kinetically favors molecular adsorption. The molecular dynamics simulations of the semiconductor-water interface confirms that this interpretation also holds for the interface with liquid water. The dynamics results show considerable agreement with the gas-phase calculations with respect to the energetics and binding-site dependence, although the lowest-energy binding configuration for gas-phase adsorption on the surface mixed dimer is outcompeted by energetically and entropically favored hydrogen bonding with the liquid.

When any amount of chemisorbed oxygen is present at the surface, water dissociation becomes strongly exothermic, and a low-barrier pathway for dissociative water adsorption becomes possible. In the gas phase, dissociation occurs via direct proton transfer to the oxygen adsorbate. However, addition of liquid water enables a second pathway which is apparently even more favorable, involving proton transfer across Grotthuss chains. Surprisingly, this mechanism is reversible within the timescale of the simulation dynamics. The differences between gas-phase and liquid water adsorption on oxygen-rich surfaces owes to the formation of hydrogen bonds with the liquid, which can substantially alter the energy landscape. We note that the equilibrium of Equation 2 will shift further upon changes to the pH or upon application of an external bias potential, which we do not consider here.

Our results suggest that under device operation, dissociative adsorption of liquid water at surface oxygen sites should lead to a self-sustaining surface hydroxylation process that will activate even at relatively small initial surface oxygen concentrations. Because this process effectively converts surface oxygen to surface hydroxyl, we propose that an initially hydroxylated surface will be an effective model for future study. We do so without loss of generality, since the initially oxygen-rich surface and an initially hydroxyl-rich surface are expected to be very similar once the interface has fully equilibrated.

VI. ACKNOWLEDGMENTS

The authors acknowledge helpful discussions with J. Turner, T. Deutsch, and H. Wang (NREL). Funding was provided by the U.S. Department of Energy Fuel Cell Technologies Program. Computing support came from the Lawrence Livermore National Laboratory (LLNL) Institutional Computing Grand Challenge program. This work was performed under the auspices of the U.S. Department of Energy by LLNL under Contract DE-AC52-07NA27344.

- ¹U.S. Department of Energy, DOE BESAC Report (2008).
- ²N. S. Lewis and D. G. Nocera, PNAS **103**, 15729 (2006).
- ³J. Turner *et al.*, Int. J. Energy Res. **32**, 379 (2008).
- ⁴O. Khaselev and J. A. Turner, Science **280**, 425 (1998).
- ⁵S. Menezes, B. Miller, and K. J. Bachmann, J. Vac. Sci. Technol. B **1**, 48 (1983).
- ⁶H. Lewerenz and K. Schulte, Electrochim. Acta **47**, 2639 (2002).
- ⁷J. Vigneron, M. Herlem, E. M. Khoumri, and A. Etcheberry, Appl. Surf. Sci. **201**, 51 (2002).
- ⁸H. Wang and J. A. Turner, ECS Trans. **2**, 125 (2007).
- ⁹T. G. Deutsch, C. A. Koval, and J. A. Turner, J. Phys. Chem. B **110**, 25297 (2006).
- ¹⁰T. G. Deutsch, J. L. Head, and J. A. Turner, J. Electrochem. Soc. **155**, B903 (2008).
- ¹¹N. Gayathri, S. Izvekov, and G. A. Voth, J. Chem. Phys. **117**, 872 (2002).
- ¹²S. Jeon, H. Kim, W. A. Goddard III, and H. A. Atwater, J. Phys. Chem. C **116**, 17604 (2012).
- ¹³A. B. Muñoz García and E. A. Carter, J. Am. Chem. Soc. **134**, 13600 (2012).
- ¹⁴V. M. Bermudez, J. Appl. Phys. **113**, 184906 (2013).

- ¹⁵O. Pluchery, Y. J. Chabal, and R. L. Opila, *J. Appl. Phys.* **94**, 2707 (2003).
- ¹⁶H. Morota and S. Adachi, *J. Appl. Phys.* **100**, 054904 (2006).
- ¹⁷B. Kaiser, D. Fertig, J. Ziegler, J. Klett, S. Hoch, and W. Jaegermann, *Chem. Phys. Chem.* **13**, 3053 (2012).
- ¹⁸M. M. May, O. Supplie, C. Höhn, W.-D. Zabka, H.-J. Lewerenz, R. van de Krol, and T. Hannappel, *Proc. of SPIE* **8822**, 88220M (2013).
- ¹⁹A. Heller, *Science* **223**, 1141 (1984).
- ²⁰W. E. Spicer, I. Lindau, P. Skeath, C. Y. Su, and P. Chye, *Phys. Rev. Lett.* **44**, 420 (1980).
- ²¹H. J. Lewerenz, D. E. Aspnes, B. Miller, D. L. Malm, and A. Heller, *J. Am. Chem. Soc.* **104**, 3325 (1982).
- ²²G. Chen, S. B. Visbeck, D. C. Law, and R. F. Hicks, *J. Appl. Phys.* **91**, 9362 (2002).
- ²³B. C. Wood, T. Ogitsu, and E. Schwegler, *J. Photon. Energy* **1**, 016002 (2011).
- ²⁴B. C. Wood, T. Ogitsu, and E. Schwegler, *J. Chem. Phys.* **136**, 064705 (2012).
- ²⁵B. C. Wood, E. Schwegler, W. I. Choi, and T. Ogitsu, *J. Am. Chem. Soc.*, in press (2013).
- ²⁶R. Car and M. Parrinello, *Phys. Rev. Lett.* **55**, 2471 (1985).
- ²⁷Giannozzi, P. *et al.*, *J. Phys. Condens. Matt.* **21**, 395502 (2009).
- ²⁸D. Vanderbilt, *Phys. Rev. B* **41**, 7892 (1990).
- ²⁹J. P. Perdew, K. Burke, and M. Ernzerhof, *Phys. Rev. Lett.* **77**, 3865 (1996).
- ³⁰Y. Zhao and D. G. Truhlar, *J. Chem. Theory Comput.* **1**, 415 (2005).
- ³¹J. C. Grossman, E. Schwegler, E. W. Draeger, F. Gygi, and G. Galli, *J. Chem. Phys.* **120**, 300 (2004).
- ³²G. J. Martyna, M. L. Klein, and M. E. Tuckerman, *J. Chem. Phys.* **97**, 2635 (1992).
- ³³M. Otani and O. Sugino, *Phys. Rev. B* **73**, 115407 (2006).
- ³⁴W. L. Jorgensen, J. Chandrasekhar, J. D. Madura, R. W. Impey, and M. L. Klein, *J. Chem. Phys.* **79**, 926 (1983).
- ³⁵W. G. Schmidt, *Appl. Phys. A* **75**, 89 (2002).
- ³⁶W. M. Haynes, ed., *CRC Handbook of Chemistry and Physics*, 94th ed. (CRC Press, 2013).
- ³⁷L. A. Curtiss, D. J. Frurip, and M. Blander, *J. Chem. Phys.* **71**, 2703 (1979).
- ³⁸S. J. Suresh and V. M. Naik, *J. Chem. Phys.* **113**, 9727 (2000).
- ³⁹D. Marx, *ChemPhysChem* **7**, 1848 (2006).
- ⁴⁰M. A. Henderson, *Surf. Sci. Rep.* **46**, 1 (2002).
- ⁴¹K. C. Hass, W. F. Schneider, A. Curioni, and W. Andreoni, *Science* **282**, 265 (1998).
- ⁴²S.-C. Li, Z. Zhang, D. Sheppard, B. D. Kay, J. M. White, Y. Du, I. Lyubinetsky, G. Henkelman, and Z. Dohnálek, *J. Am. Chem. Soc.* **130**, 9080 (2008).
- ⁴³H. S. Kato, K. Akagi, S. Tsuneyuki, and M. Kawai, *J. Phys. Chem. C* **112**, 12879 (2008).
- ⁴⁴G. Cicero, G. Galli, and A. Catellani, *J. Phys. Chem. B* **108**, 16518 (2004).
- ⁴⁵J. Wang, L. S. Pedroza, A. Poissier, and M. V. Fernandez-Serra, *J. Phys. Chem. C* **116**, 14382 (2012).
- ⁴⁶C. Sun, L.-M. Liu, A. Selloni, G. Q. M. Lu, and S. C. Smith, *J. Mater. Chem.* **20**, 10319 (2010).
- ⁴⁷S. Meng, E. G. Wang, and S. Gao, *Phys. Rev. B* **69**, 195404 (2004).
- ⁴⁸J. Carrasco, A. Hodgson, and A. Michaelides, *Nature Mater.* **11**, 667 (2012).
- ⁴⁹L. R. Merte, G. Peng, R. Bechstein, F. Riebolt, C. A. Farberow, L. C. G. ans W. Kudernatsch, S. Wendt, E. Lægsgaard, M. Mavrikakis, and F. Besenbacher, *Science* **336**, 889 (2012).
- ⁵⁰N. Marzari, A. A. Mostofi, J. R. Yates, I. Souza, and D. Vanderbilt, *Rev. Mod. Phys.* **84**, 1419 (2012).
- ⁵¹S. F. Boys, *Rev. Mod. Phys.* **32**, 296 (1960).
- ⁵²O. Henrion, A. Klein, and W. Jaegermann, *Surf. Sci.* **457**, L337 (2000).
- ⁵³M. M. May, O. Supplie, C. Höhn, R. van de Krol, H.-J. Lewerenz, and T. Hannappel, arXiv:1305.5815 [cond-mat.mtrl-sci] (2013).
- ⁵⁴O. Khaselev and J. A. Turner, *J. Electrochem. Soc.* **145**, 3335 (1998).
- ⁵⁵S. Menezes, H. J. Lewerenz, F. A. Thiel, and K. J. Bachmann, *Appl. Phys. Lett.* **38**, 710 (1981).
- ⁵⁶A. Heller, B. Miller, H. J. Lewerenz, and K. J. Bachmann, *J. Am. Chem. Soc.* **102**, 6555 (1980).